Ultramicroscopy 110 (2010) 582–585

Contents lists available at ScienceDirect

Ultramicroscopy

journal homepage: www.elsevier.com/locate/ultramic

Multifrequency high-speed phase-modulation atomic force microscopy in liquids

Yan Jun Li*, Kouhei Takahashi, Naritaka Kobayashi, Yoshitaka Naitoh, Masami Kageshima, Yasuhiro Sugawara

Department of Applied Physics, Graduate School of Engineering, Osaka University, 2-1 Yamada-oka, Suita, Osaka 565-0871, Japan

ARTICLE INFO

Keywords:
Multifrequency
High-speed phase modulation
Atomic force microscopy
Elasticity

ABSTRACT

We have developed a new technique, called multifrequency high-speed phase-modulation atomic force microscopy (PM-AFM) in constant-amplitude (CA) mode based on the simultaneous excitation of the first two flexural modes of a cantilever. By performing a theoretical investigation, we have found that this technique enables the simultaneous imaging of the surface topography, energy dissipation and elasticity (nonlinear mapping) of materials. We experimentally demonstrated high-speed imaging at a scan speed of 5 frames/s for a polystyrene (PS) and polyisobutylene (PIB) polymer-blend thin-film surface in water.

1. Introduction

The atomic force microscope (AFM) [1–7] is a powerful tool for observing various surfaces with high spatial resolution at the nanometerscale in various environments. In particular, high-speed AFM can be used to directly observe the dynamical behavior of biomolecular processes involving DNA, proteins and living cells in real time with a millisecond timescale [8]. When high-speed AFM is operated in the amplitude-modulation (AM) mode, which is based on the tapping mode, soft biomaterials in liquids are damaged by the strong tip–sample interaction forces and instability in the cantilever dynamics is another problem. Thus, the enhancement of force sensitivity and the removal of instability are required to achieve for next-generation high-speed AFM.

In a previous paper [9], we theoretically and experimentally clarified that phase-modulation (PM) AFM has higher force sensitivity than AM-AFM. Actually, true atomic resolution is demonstrated in liquid using PM-AFM by Fukuma et al. [33]. Furthermore, we have proposed a new operation mode, "PM-AFM in constant-amplitude (CA) mode," to prevent instability in the cantilever dynamics [10]. In this mode, the cantilever is driven by an oscillator signal through an oscillating control amplifier, which is equipped with an automatic gain control (AGC) circuit to keep the oscillation amplitude constant. The phase shift ($\delta\phi_1$) is used as a feedback signal to image the sample topography. This new operation mode has several advantages compared with AM-AFM: (i) higher force sensitivity, (ii) no instability in the cantilever dynamics, (iii) a continuous force curve for the full range of tip–sample force curve and (iv) the capability of compensating for the fluctuation of the cantilever-excitation efficiency due to thermal drift in liquids. This new operation mode also has several advantages compared with frequency-modulation (FM) AFM [11–13]: (i) no stoppage oscillation because of the external driving of the cantilever by the oscillator and (ii) rapid detection of the phase shift because a fast phase detector is used instead of a slow phase-locked loop (PLL) circuit. On the basis of above-mentioned advantages, we have developed high-speed PM-AFM in CA mode as a next-generation high-speed AFM technique that is superior to AM-AFM and FM-AFM [14,15].

Material properties are very important information that can be obtained from energy dissipation. In our proposed technique of high-speed PM-AFM in CA mode, the energy dissipation is measured from the excitation amplitude (A_{exc}) of the cantilever as the dissipative (nonconservative) interaction between the oscillating tip and the surface, which is strongly related to the viscosity of the sample surface [14]. The conservative interaction between the tip and surface also provides important information on the sample surface related to its elasticity, but a method for measuring this interaction has not yet been developed for PM-AFM in CA mode. Thus, to image soft biological samples with material contrast, a new operation mode based on the high-speed PM-AFM in CA mode is needed.

Recently, the higher harmonics [16–20] and modes [21–27,34,35] to enhance the sensitivity to tip–sample interactions have been proposed in several studies. In particular, the bimodal dynamic AM-AFM has been proposed by Rodriguez and Garcia et al. [24] which consists of the simultaneous excitation of the two modes of the cantilever, usually the first and the second

* Corresponding author.
E-mail address: liyanjun@ap.eng.osaka-u.ac.jp (Y. Jun Li).

0304-3991/$ - see front matter © 2010 Elsevier B.V. All rights reserved.
doi:10.1016/j.ultramic.2010.02.014

modes. It is suggested from theory, numerical simulations and experiments that this method is more sensitive to the material contrast at low forces than conventional monomodal AM-AFM. The bimodal AFM by using the second mode can give the origin of the material contrast (phase shift $\delta\phi_2$) due to the ability to detect conservative and nonconservative interactions separately [27]. In the operation of FM-AFM using higher flexural modes of the cantilever, the current trend is to reduce free oscillation amplitude (A0) [28]. Actually, in the higher harmonics, with low quality factors, it is expected that there is significant energy by Xu et al. [34] and local elastic has been imaged by Melcher et al. [35] in liquids.

In this paper, we develop a new technique of multifrequency high-speed PM-AFM in CA mode which is based on the simultaneous excitation of two flexural modes of the cantilever (the first and second). This new technique provides two additional information channels compared‘ with conventional monomodal PM-AFM operation. Namely, the simultaneous excitation signal enables the number of information channels to be increased from two to four, the signals of the amplitudes and phase shifts of the first and second flexural modes. We discuss this technique from both theoretical and experimental viewpoint and demonstrate the capability of simultaneously imaging the topography, energy dissipation and elasticity of a polymer-blend film surface in water.

2. Theoretical model

Here, let us consider the theory of multifrequency PM-AFM in CA mode. Similarly to the theory of bimodal AM-AFM [26], we obtain a system with two differential equations for the motion of the cantilever as follows:

$$m\ddot{z}_1+\frac{m\omega_2}{Q_2}\dot{z}_1+k_1z_1=k_1A_{exc1}\cos\omega_1t+K_2A_{exc2}\cos\omega_2t+F_{ts} \quad (1)$$

$$m\ddot{z}_2+\frac{m\omega_1}{Q_1}\dot{z}_2+k_2z_2=k_1A_{exc1}\cos\omega_1t+K_2A_{exc2}\cos\omega_2t+F_{ts}. \quad (2)$$

Here, m and F_{ts} are the effective mass and the nonlinear tip-surface interaction, respectively. ki, z_i, $\omega_i=2\pi f_i=\sqrt{k_i/m}$, A_{exci} and Q_i are the spring constant, the deflection of the cantilever, the resonant frequency, the oscillation amplitude and the natural Q-factor of the cantilever in the first and second modes, respectively. Note that if we do not consider the term representing the contribution of the other harmonics and modes, the cantilever deflection signal $z(t)$ as a function of time t in the steady state is given by

$$z(t)\approx A_1\cos(\omega_1t-\pi/2-\delta\phi_1)+A_2\cos(\omega_2t-\pi/2-\delta\phi_2) \quad (3)$$

Here, z includes a term z_1 in the first mode and a term z_2 in the second mode and $\delta\phi_i$ is the phase shift between the external excitation and the oscillation of the cantilever in the first and second modes. Inserting Eq. (3) into Eqs. (1) and (2), multiplying both sides of Eqs. (1) and (2) by $\cos(\omega_1t-\pi/2-\delta\phi_1)$, $\sin(\omega_2t-\pi/2-\delta\phi_2)$, respectively, then integrating over the oscillation period $T=2\pi/\omega_i$ we obtain the following four equations:

$$k_1A_{exc1}\sin\delta\phi_1=\frac{2}{T}\int_0^T F_{ts}\cos\left(\omega_1t-\frac{\pi}{2}-\delta\phi_1\right)dt \quad (4)$$

$$k_1A_{exc1}\cos\delta\phi_1=\frac{k_1A_1}{Q_1}+\frac{2}{T}\int_0^T F_{ts}\sin\left(\omega_1t-\frac{\pi}{2}-\delta\phi_1\right)dt \quad (5)$$

$$k_2A_{exc2}\sin\delta\phi_2=\frac{2}{T}\int_0^T F_{ts}\cos\left(\omega_2t-\frac{\pi}{2}-\delta\phi_2\right)dt \quad (6)$$

$$k_2A_{exc2}\cos\delta\phi_2=\frac{k_2A_2}{Q_2}+\frac{2}{T}\int_0^T F_{ts}\sin\left(\omega_2t-\frac{\pi}{2}-\delta\phi_2\right)dt \quad (7)$$

Here, F_{c2} and F_{d2} are defined by $F_{c2}=\frac{2}{T}\int_0^T F_{ts}\cos(\omega_2t-\pi/2-\delta\phi_2)dt$, and$F_{d2}=\frac{2}{T}\int_0^T F_{ts}\sin(\omega_2t-\pi/2-\delta\phi_2)dt$ which are conservative and nonconservative tip–sample interactions in the second mode, respectively. From Eqs. (6) and (7), we can obtain Eq. (8), with the relationship for the phase shift at the second mode as follows:

$$\tan\delta\phi_2=\frac{\sin\delta\phi_2}{\cos\delta\phi_2}=\frac{F_{c2}}{K_2A_2/Q_2+F_{d2}} \quad (8)$$

Here, it is assumed that the conservative force is dominant in PM-AFM in CA mode, $F_{d2}\approx0$, because the first phase shift is kept constant as a feedback signal. Because F_{c2} is equal to the difference between all conservative forces F_c and the conservative force F_{c1} in the first mode, Eq. (8) can be rewritten to the following expression (9).

$$\tan\delta\phi_2\approx\frac{Q_2}{K_2A_2}F_{c2}=\frac{Q_2}{K_2A_2}(F_c-F_{c1}) \quad (9)$$

In PM-AFM in CA mode, F_{c1} is almost constant. Thus, the change of F_c contributes to the phase shift $\delta\phi_2$ in the second mode. Namely, we can nonlinear map elasticity of the sample surface from the phase shift $\delta\phi_2$ in the second mode.

3. Experimental setup

In multifrequency high-speed PM-AFM in CA mode, two additional information channels are provided that are not available in monomodal high-speed PM-AFM operation in CA mode [14,15]. The simultaneous excitation signal enables the number of information channels to be increased from two (A_1,$\delta\phi_1$) to four, i.e., the signals of the amplitudes (A_1, A_2) and phase shifts ($\delta\phi_1$, $\delta\phi_2$) of the first and second flexural modes. Fig. 1 shows the experimental setup of multifrequency high-speed PM-AFM in the CA mode. The cantilever is driven by an oscillator signal with frequency f_1 (600 kHz) in the first mode and frequency f_2 (3 MHz) at the second mode. The cantilever is driven by photothermal excitation. The deflection signal of the cantilever is divided into two signals by a band-pass filter. In the first mode, the oscillating control amplifier is equipped with AGC circuit, which keeps the oscillation amplitude A_1 constant. The amplitude A_1 and the phase ϕ_1 of the oscillating cantilever relative to the oscillator signal are detected by high-speed amplitude and phase detector using the sample and hold (S/H) technique [29]. The phase shift ϕ_1 is used as a feedback signal to image the sample topography. The energy dissipation can be measured from the amplitude A_{exc1} of the cantilever-excitation signal from the AGC circuit. In the second mode, the phase shift ϕ_2 is used to image the elasticity of the sample surface, which is also measured by a high-speed phase detector using the S/H technique [29–31].

4. Samples and sensors

To evaluate the performance of our apparatus carrying out multifrequency high-speed PM-AFM in CA mode in water, we used a polymer-blend film of polystyrene (PS, Young’s modulus: approximately 3 GPa) and polyisobutylene (PIB, Young’s modulus: approximately 3 MPa). Because PS is in a glassy state and PIB is in rubbery state at room temperature, the polymer-blend film can provide a different contrast. Also, this film should be suitable for the analysis of elasticity images. In addition, such films have widely been used in AFM experiments [32].

As a force sensor, we used a special cantilever (Olympus Bio-Level mini) made from silicon nitride with an Au-coated thin film on the back surface. This Au-coated thin film serves as a metal coating for enabling photothermal excitation as well as the optical

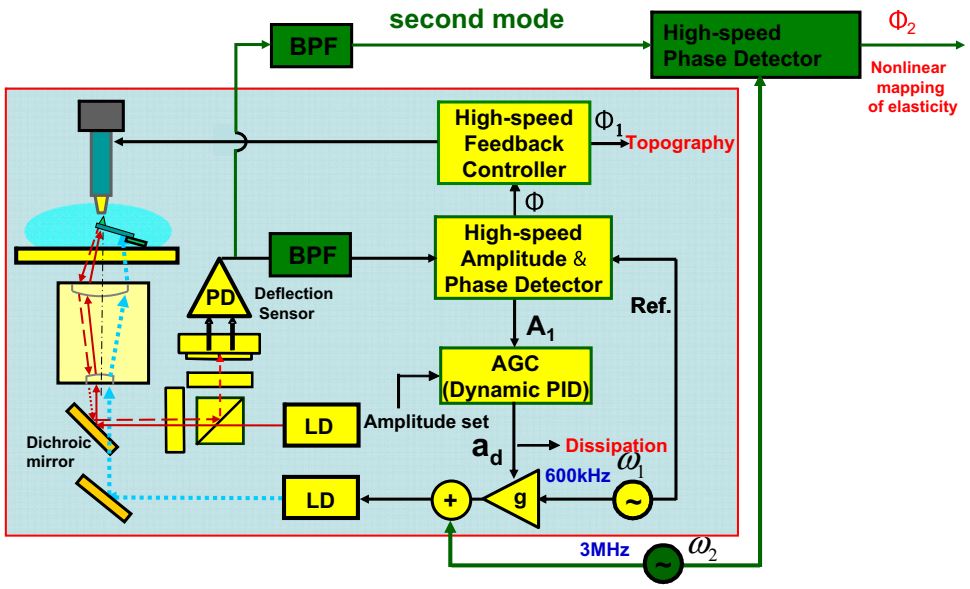

Fig. 1. Block diagram of multifrequency high-speed PM-AFM in CA mode. Here, the red box represents monomodal high-speed PM-AFM in CA mode and the green box represents PM-AFM in the second mode. (For interpretation of the references to colour in this figure legend, the reader is referred to the web version of this article.)

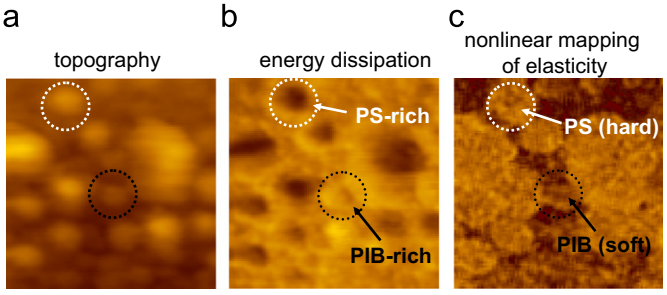

Fig. 2. (a) Topography, (b) energy dissipation and (c) nonlinear mapping of elasticity measured by multifrequency high-speed PM-AFM in CA mode performed on polymer-blend thin film composed of PS and PIB. The scanning area was $300 \times 300\ \text{nm}^2$. The scan speed was 5 frames/s.

detection of cantilever deflection. The spring constant is 0.2 N/m, the resonance frequency is 1500 kHz in air and 600 kHz in water and the Q-factor is approximately 5 in water. The length, width and thickness of the cantilever were 8 μm, 2 μm and 0.13 μm, respectively. The amplitude A_1 and phase shift ϕ_1 of the oscillating cantilever were set to approximately 10 nm and -3°, respectively.

5. Experimental results

Fig. 2(a)–(c) show topographic, energy dissipation and elasticity images of the PS/PIB polymer surface measured by multifrequency high-speed PM-AFM in CA mode, respectively. The scanning area is $300 \times 300\ \text{nm}^2$ and the Scan speed is 5 frames/s. In the topographic image in Fig. 2(a), we can observe islands of different size and approximately the same bright contrast. Here, it is difficult to identify the difference between PS-rich and PIB-rich regions, because these islands do not exhibit a material-specific contrast. However, in the energy dissipation image in Fig. 2(b), the regions of hard glassy PS and soft rubbery PIB are clearly exhibited as dark and bright contrast, respectively. Furthermore, the contrast of hard glassy PS, which has a large phase shift, is brighter than that of soft rubbery PIB, which has a small phase shift in elasticity image (nonlinear mapping) shown in Fig. 2(c). Thus, our proposed technique of multifrequency high-speed PM-AFM in CA mode is useful for demonstrating the elasticity of the polymer-blend surface. Namely, it has the ability to simultaneously image the topography, energy dissipation and nonlinear mapping of elasticity. Furthermore, our results are in agreement with a previous report by Tamayo and García [7].

Fig. 3(a)–(c) show the topography, energy dissipation and nonlinear mapping of elasticity of a different area on the same surface, respectively and Fig. 3(a′), (b′) and (c′) are the corresponding line profiles. The scanning area is $300 \times 300\ \text{nm}^2$. The scan speed is 1 frame/s. From the topographic and energy dissipation images, it is difficult to conclude that areas I and II are made of the same material owing to their different heights (see Fig. 3(a′) and (b′)). However, Figs. 3(c) and (c′)), we can see that areas I and II have almost the same contrast and height. Hence, it is easy to judge that areas I and II are made of the same material. Therefore, nonlinear mapping of elasticity contains different information on the material compared with the topographic and energy dissipation images.

6. Conclusions

We have developed a technique of high-speed phase-modulation (PM) atomic force microscopy (AFM) in constant-amplitude (CA) mode in liquids based on the simultaneous excitation of the first two flexural modes of the cantilever, which we call multi-frequency high-speed PM-AFM in CA mode. We have discussed this technique from a theoretical viewpoint and have demonstrated the applicability of this new technique by imaging the elasticity of a polymer-blend film with a scan speed of 5 frames/s in water. Multifrequency high-speed PM-AFM in CA mode is more sensitive to material contrast than monomodal high-speed PM-AFM in CA mode. Namely, the phase shift of the second flexural mode is a very important parameter that gives very high elasticity contrast between different materials. This technique is expected to be widely used in many fields. In the near future, we

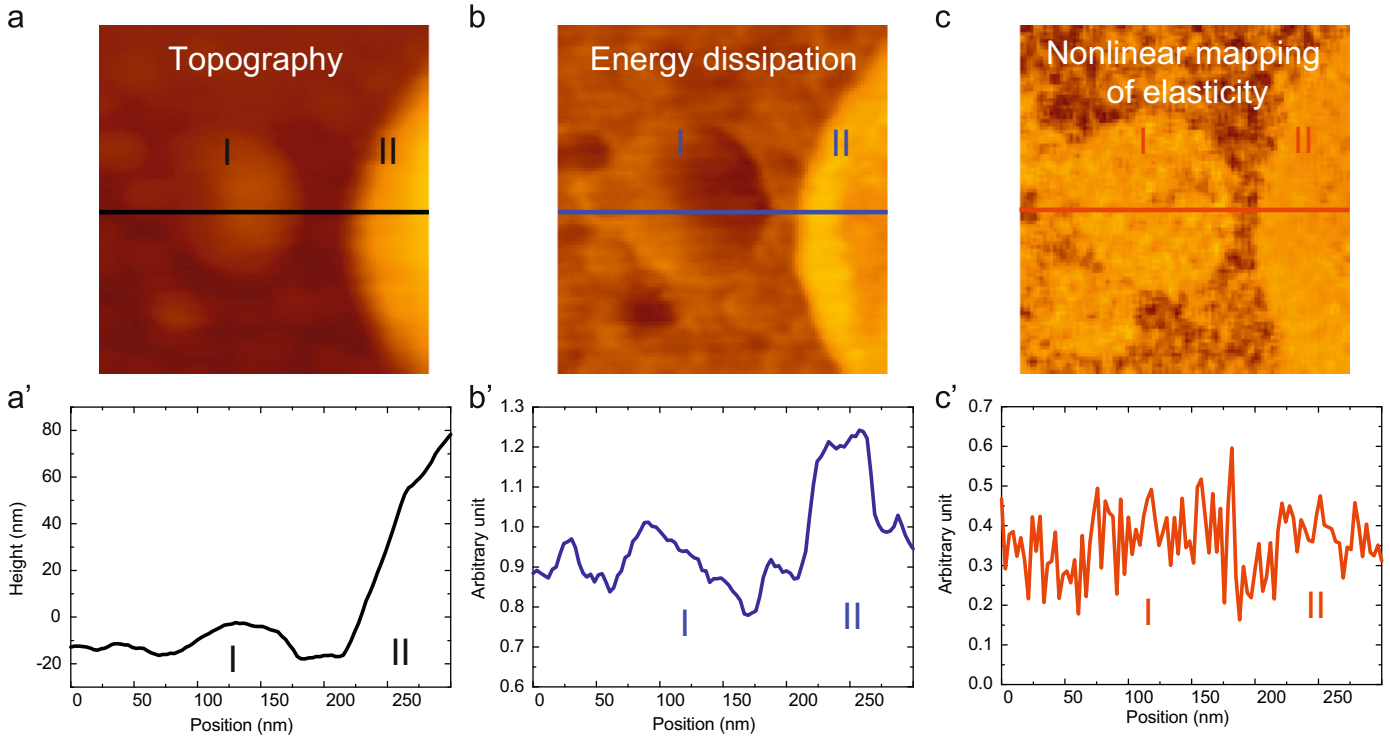

Fig. 3. (a) Topography, (b) energy dissipation and (c) nonlinear mapping of elasticity of polymer-blend thin film composed of PS and PIB. (a′), (b′) and (c′) are the line profiles corresponding to (a), (b) and (c). The scanning area was $300 \times 300\ nm^2$. The scan speed was 1 frame/s.

plan to obtain a true atomic resolution at a video rate using this technique.

Acknowledgements

The authors acknowledge support from CREST, Japan Science and Technology Agency and a Grant-in-Aid for Scientific Research from the Ministry of Education, Culture, Sports, Science and Technology of Japan.

References

[1] G. Binnig, C.F. Quate, Ch. Gerber, Phys. Rev. Lett. 56 (1986) 930–933.
[2] Y. Martin, C.C. Williams, H.K. Wickramasinghe, J. Appl. Phys. 61 (1987) 4723–4729.
[3] T.R. Albrecht, P. Grütter, D. Horne, D. Rugar, J. Appl. Phys. 69 (1991) 668–673.
[4] Q. Zhong, D. Inniss, K. Kjoller, V.B. Elings, Surf. Sci. 290 (1993) L688–L692.
[5] C. Bustamante, D.A. Erie, D. Keller, Curr. Opin. Struct. Biol. 4 (1994) 750–760.
[6] P.K. Hansma, J.P. Cleveland, M. Radmacher, D.A. Walters, P.E. Hillner, M. Bezanilla, M. Fritz, D. Vie, H.G. Hansma, C.B. Prater, J. Massie, L. Fukunaga, J. Gurley, V. Elings, Appl. Phys. Lett. 64 (1994) 1738–1740.
[7] J. Tamayo, R. García, Langmuir 12 (1996) 4430–4435.
[8] T. Ando, N. Kodera, E. Takai, D. Maruyama, K. Saito, A. Toda, Proc. Natl. Acad. Sci. USA 98 (2001) 12468–12472.
[9] N. Kobayashi, Y.J. Li, Y. Naitoh, M. Kageshima, Y. Sugawara, Jpn. J. Appl. Phys. 45 (2006) L793–L795.
[10] Y. Sugawara, N. Kobayashi, M. Kawakami, Y.J. Li, Y. Naitoh, M. Kageshima, Appl. Phys. Lett. 90 (2007) 194104-1–194104-3.
[11] H. Hölscher, Appl. Phys. Lett. 89 (2006) 123109-1–123109-3.
[12] M. Lee, W. Jhe, Phys. Rev. Lett. 97 (2006) 036104-1–036104-4.
[13] R. García, A.S. Paulo, Phys. Rev. B 60 (1999) 4961–4967.
[14] Y.J. Li, N. Kobayashi, H. Nomura, Y. Naitoh, M. Kageshima, Y. Sugawara, Jpn. J. Appl. Phys. 47 (2008) 6121–6124.
[15] Y.J. Li, N. Kobayashi, Y. Naitoh, M. Kageshima, Y. Sugawara, Appl. Phys. Lett. 92 (2008) 121903-1–121903-3.
[16] J. Legleiter, T. Kowalewski, Appl. Phys. Lett. 87 (2005) 163120-1–163120-3.
[17] J. Preiner, J. Tang, V. Pastushenko, P. Hinterdorfer, Phys. Rev. Lett. 99 (2007) 046102-1–046102-4.
[18] O. Sahin, C.F. Quate, O. Solgaard, A. Atalar, Phys. Rev. B 69 (2004) 165416-1–165416-9.
[19] M. Stark, R.W. Stark, W.M. Heckl, R. Guckenberger, Appl. Phys. Lett. 77 (2000) 3293–3295.
[20] S. Crittenden, A. Raman, R. Reifenberger, Phys. Rev. B 72 (2005) 235422-1–235422-13.
[21] D.W. Dareing, T. Thundat, S. Jeon, M. J. Nicholson. J. Appl. Phys. 97 (2005) 084902-1–084902-6.
[22] S.C. Minne, S.R. Manalis, A. Atalar, C.F. Quate, Appl. Phys. Lett. 68 (1996) 1427–1429.
[23] Y. Sugimoto, S. Innami, M. Abe, O. Custance, S. Morita, Appl. Phys. Lett. 91 (2007) 093120-1–093120-3.
[24] T.R. Rodríguez, R. García, Appl. Phys. Lett. 84 (2004) 449–451.
[25] J.R. Lozano, R. García, Phys. Rev. Lett. 100 (2008) 076102-1–076102-4.
[26] N.F. Mart′inez, J.R. Lozano, E.T. Herruzo, F. García, C. Richter, T. Sulzbach, R. Garccía Nanotechnology 19 (2008) 384011-1–384011-8.
[27] S. Kawai, S. Kitamura, S. Meguro, H. Kawakatsu, Appl. Phys. Lett. 86 (2005) 193107-1–193107-3.
[28] S. Kawai, H. Kawakatsu, Appl. Phys. Lett. 88 (2006) 133103-1–133103-3.
[29] A.D.L. Humphris, M.J. Miles, J.K. Hobbs, Appl. Phys. Lett. 86 (2005) 034106-1–034106-3.
[30] T. Uchihashi, T. Ando, H. Yamashita, Appl. Phys. Lett. 89 (2006) 213112-1–213112-3.
[31] M. Stark, R. Guckenberger, Rev. Sci. Instrum. 70 (1999) 3614–3619.
[32] H. Nukaga, S. Fujinami, H. Watabe, K. Nakajima, T. Nishi, Jpn. J. Appl. Phys. 44 (2005) 5425–5429.
[33] T. Fukuma, J.I. Kilpatrick, S.P. Jarvis, Rev. Sci. Instrum. 77 (2006) 123703-1–123703-5.
[34] X. Xu, J. Melcher, S. Basak, R. Reifenberger, A. Raman, Phys. Rev. Lett. 102 (2009) 060801-1–060801-4.
[35] J. Melcher, C. Carrasco, X. Xu, J.L. Carrascosa, J. Gómez-Herrero, P.J. Pablo, A. Raman, Proc. Natl. Acad. Sci. USA. 106 (2009) 13655–13660.